This version is available at https://strathprints.strath.ac.uk/66092/

Heat and mass transfer of oscillatory lid-driven cavity flow in the continuum, transition and free molecular flow regimes

Peng Wang, Wei Su, Lianhua Zhu, Yonghao Zhang *

James Weir Fluids Laboratory, Department of Mechanical and Aerospace Engineering, University of Strathclyde, Glasgow G1 1XJ, UK

ABSTRACT

Although effective cooling of micro-electro-mechanical systems (MEMS) with oscillatory components is essential for reliable device operation, the role of oscillation on heat transfer remains poorly understood. In this work, heat and mass transfer of the oscillatory gas flow inside a square cavity is computationally studied by solving the Boltzmann model equation, i.e. the Shakhov model. The oscillation frequency of the lid and rarefaction and nonlinearity of the flow field are systematically investigated. Our results show that, when the oscillation frequency of the lid increases, the usual cold-to-hot heat transfer pattern for highly rarefied flow changes to hot-to-cold, which contradicts the well-known anti-Fourier (i.e. cold-to-hot) heat transfer in a non-oscillatory lid-driven cavity. In addition, the thermal convection will be dramatically enhanced by lid oscillation, which may play a dominant role in the heat transfer. Meanwhile, the average Nusselt number varies non-monotonically with the oscillation frequency, with the maximum occurring at the anti-resonance frequency. Finally, the average Nusselt number on the lid at various oscillation frequencies is found to reduce when the gas becomes more rarefied. These findings may be useful for the thermal design of MEMS.

1. Introduction

The micro-oscillators are commonly built in the micro-electro-mechanical system (MEMS) devices [1], e.g. the micro-accelerometers, the inertial sensors, and the resonating sensors. Proper cooling of the oscillatory components is key to the reliable and robust operation of MEMS devices. However, heat transfer in the MEMS oscillators remains poorly understood.

With the miniaturization of the device structure, the characteristic dimension could shrink to the micro- and nano-scales, in which the gas flows are generally rarefied. The degree of gas rarefaction is normally characterized by the Knudsen number (Kn), which is defined as the ratio of the gas mean free path to the characteristic flow length. Alternatively, the Knudsen number can also be defined as the ratio of the oscillation frequency and the mean collision frequency of gas molecules [2]. The most gas MEMS devices operate in the slip ($10^{-3} \lesssim Kn \lesssim 0.1$) and early transition regimes ($0.1 \lesssim Kn \lesssim 1$) [3,4]. Furthermore, the oscillation frequency of the moving parts may aggravate non-equilibrium of gas flow in oscillatory systems [5,6]. As the conventional Navier-Stokes-Fourier equations break down, the gas kinetic theory should be adopted for rarefied flow analysis [7,8].

The oscillatory rarefied gas flows have been investigated by seeking the solutions of the Boltzmann equation and its model equations, which are usually solved by the direct simulation Monte Carlo (DSMC) method [3,9–14] or the discrete velocity method (DVM) [4,5,2,7,15–17]. These studies have been focused on the damping force on the oscillating parts, the effect of oscillation on heat transfer for rarefied flows has largely been oversighted [11,12], except for simple one-dimensional (1D) oscillating Couette flows [11,18]. Note that great efforts have been made to investigate the heat transfer in non-oscillatory rarefied lid-driven cavity flows [19–23], in which the non-Fourier heat transfer (i.e., the cold-to-hot heat flux) was reported, and the effect of external force field on heat transfer was also discussed [21,22].

For the DSMC and DVM methods, the computational time step and spatial mesh size need to be smaller than the mean collision time and the gas mean free path, respectively, if the free streaming and collisions of gas molecules are dealt with separately. Thus, these two methods are computationally expensive for flows near the hydrodynamic regime [24,25]. As a result, studies of the oscillatory rarefied gas flows are mainly restricted in the highly rarefied regimes. Meanwhile, the velocity amplitude of the oscillator is usually assumed to be very small, so that the linearized Boltzmann equation or its model equations can be used to obtain the analytical results for the simple 1D flows in the limits of the continuum and free molecular regimes [2,26]. In fact, the velocity magnitude

---

of the oscillator can also dramatically affect the mass and heat transfer [16,27,6]. Therefore, it is necessary to take account of the effect of flow nonlinearity/compressibility in studying the heat transfer of the oscillatory flows.

Recently, we used the discrete unified gas-kinetic scheme (DUGKS) to solve the gas kinetic model for an oscillatory rarefied cavity flow focusing on the damping force exerting on the oscillatory lid [6,28]. In this work, the flow and thermal characteristics of the oscillatory rarefied gas flow inside a square cavity are investigated on the basis of the Shakhov equation. The effects of gas nonlinearity and oscillation frequency are systematically studied covering the flow regimes from the hydrodynamic to free molecular flows. The results of non-oscillatory lid-driven rarefied cavity flow are also presented for comparison [29].

The remainder of the paper is organized as follows. We introduce the formulation of the problem and the Shakhov model in Section 2. The computational details including discretizations of the molecular velocity space, the spatial space, and the temporal space are described in Section 3. Our numerical results for mass and heat transfer are presented and discussed in Section 4, which is followed by the conclusions in Section 5.

2. Problem formulation

We consider a rarefied monatomic gas flow in a two-dimensional square cavity driven by a moving lid at $y = H$, see Fig. 1. The lid oscillates harmonically in the x-direction at frequency ω, with the velocity given by

$$U_w = U_0 \cos(\omega t), \tag{1}$$

where U_0 is the amplitude of the oscillating velocity, and t is the time. The other three walls at $x = 0, x = H$, and $y = 0$ are fixed, and all the four walls are isothermal with a fixed temperature of T_w.

The problem considered is characterized by the Mach number (Ma), the Strouhal number (St), and the Knudsen number, which are, respectively, defined as

$$Ma = \frac{U_0}{\sqrt{\gamma RT_w}}, \quad St = \frac{\omega H}{v_m}, \quad Kn = \frac{\lambda}{H}, \tag{2}$$
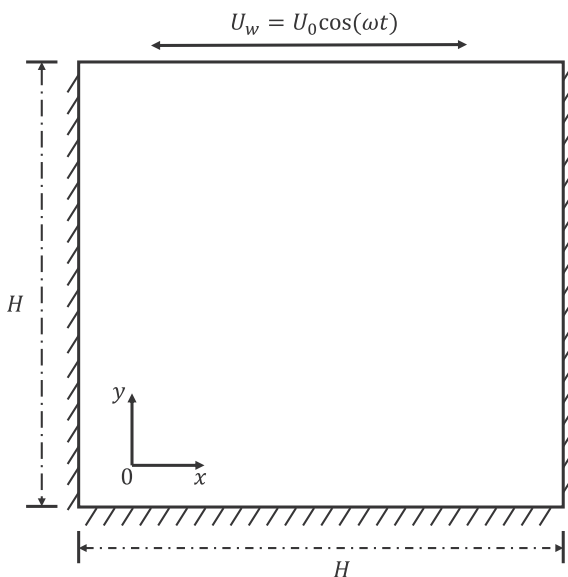

Fig. 1. Schematic diagram of the oscillatory flow in a square cavity. The origin of the coordinate is located at the left bottom corner of the cavity.

where $\gamma = 5/3$ is the specific heat ratio for monatomic gas, $v_m = \sqrt{2RT_w}$ is the most probable molecular speed with R being the specific gas constant, and λ is the mean free path of gas molecules, which is related to the shear viscosity μ of the gas as

$$\lambda = \frac{\mu(T = T_w)}{p} \frac{\sqrt{\pi} v_m}{2}, \tag{3}$$

where $p = \rho RT$ is the gas pressure, with ρ and T being the density and temperature, respectively. In this work, the hard-sphere molecular model is used, where the shear viscosity of the gas is determined by power-law in terms of the gas temperature:

$$\mu = \mu(T = T_w)\left(\frac{T}{T_w}\right)^{0.5}. \tag{4}$$

The Shakhov equation, which is widely used to describe the dynamics of monatomic gases [30], is adopted to describe the non-equilibrium flow induced by the gas rarefaction and the oscillation of the lid. In the absence of external force, it takes the form of

$$\frac{\partial f}{\partial t} + \xi \cdot \nabla f = -\frac{1}{\tau}\left[f - f^S\right], \tag{5}$$

where $f(\mathbf{x}, \xi, t)$ is the molecular velocity distribution function of gas molecules at the position $\mathbf{x} = (x, y, z)$, time t, velocity $\xi = (\xi_x, \xi_y, \xi_z)$. f^S is the reference distribution function expressed as the combination of the Maxwellian distribution function f^{eq} and a heat flux correction term:

$$f^S = f^{eq}\left[1 + (1 - Pr)\frac{\mathbf{c} \cdot \mathbf{q}}{5pRT}\left(\frac{c^2}{RT} - 5\right)\right], \tag{6}$$

where $\mathbf{c} = \xi - \mathbf{U}$ is the peculiar velocity with $\mathbf{U}$ being the macroscopic flow velocity, $\mathbf{q} = \frac{1}{2}\int \mathbf{c}c^2 f d\xi$ is the heat flux, and $Pr = c_p\mu/k$ is the Prandtl number being equal to 2/3 for the monatomic gases. Here c_p is the specific heat, μ is the dynamic viscosity, and k is the thermal conductivity. The collision time τ in Eq. (5) is given in terms of the dynamic viscosity μ and the gas pressure p as $\tau = \mu/p$. The Maxwellian distribution function f^{eq} is given by

$$f^{eq} = \frac{\rho}{(2\pi RT)^{3/2}} \exp\left(-\frac{c^2}{2RT}\right), \tag{7}$$

where ρ is the gas density.

The conservative variables $\mathbf{W} \equiv (\rho, \rho\mathbf{U}, \rho E)^T$ are calculated from the velocity moments of the velocity distribution function: $\mathbf{W} = \int \psi f d\xi$, where $\psi = \left(1, \xi, \frac{1}{2}\xi^2\right)^T$. Note that the gas temperature is related to the total gas energy as $\rho E = \frac{1}{2}\rho U^2 + \frac{3}{2}\rho RT$. In addition, the shear stress can be computed as

$$\sigma_{xy} = \int c_x c_y f d\xi, \tag{8}$$

where c_x and c_y denote the components of peculiar velocity in the x- and y-axises, respectively.

3. Numerical method

The DUGKS is used to solve the Shakhov equation [31], where the velocity distribution function across the cell interfaces is constructed on basis of the discrete characteristic solution of the kinetic model, consisting of both the kinetic and hydrodynamic parts [25,32]. With the intrinsic coupling of molecular collision and transport processes in determining the flux across the cell interface, the computational time step and mesh size are not limited by the mean collision time and mean free path of gas molecules, respectively. Therefore, the multiscale-flow physics can be efficiently and self-adaptively captured from the hydrodynamic

Table 1
Details of the discretizations in the molecular velocity space and spatial space. Here $(G/Nm, n)$ represents using m Gauss-Hermite/Nonuniform velocity points and n grid points in each direction of the molecular velocity space and spatial space, respectively. Note that the integration interval for the trapezoidal rule is truncated within $[-4v_m, 4v_m]$ and $[-6v_m, 6v_m]$ for Ma = 0.1 and 1, respectively.

Kn	0.001	0.01	0.1	1	10
$Ma = 0.1$	(G8, 64)	(G16, 48)	(G16, 32)	(N32, 32)	(N48, 32)
$Ma = 1$	(G16, 64)	(G28, 48)	(G28, 32)	(N48, 32)	(N48, 32)

to the free molecular flow regimes [24]. The details of the DUGKS for the Shakhov model can be found in Guo et al. [31].

In order to accurately approximate the moments of velocity distribution function, the continuous molecular velocity space $(\xi_x, \xi_y, \xi_z \in (-\infty, +\infty))$ should be discretized according to the degrees of rarefaction and compressibility of the gas flow, using a certain quadrature rule to compute the velocity integrals. For slightly rarefied flows with low Mach number, the highly accurate Gauss-Hermite quadrature with few discrete velocity points is usually applied, while the trapezoidal rule with more discrete velocity points associated with nonuniform abscissas [33,34] is adopted to

capture discontinuities in the distribution function for high-speed flows in the highly rarefied regimes. Details of the discretized molecular velocity space are given in Table 1.

For the spatial discretization, in order to accurately capture the flow properties near the wall boundary, a set of non-uniform meshes with $N_x \times N_y$ grid points are adopted in the x- and y-axes, respectively, and the mesh resolution is gradually refined from the cavity center to the walls. The location of a control volume center (x_i, y_j) is generated by $x_i = (\zeta_i + \zeta_{i+1})/2, y_j = (\zeta_j + \zeta_{j+1})/2$, $0 \leqslant i < N_x, 0 \leqslant j < N_y$, where ζ_i is defined by

$$\zeta_i = \frac{1}{2} + \frac{\tanh[a(i/N - 0.5)]}{\tanh(a/2)}, i = 0, 1, 2, \ldots, N_{x,y} - 1, \qquad (9)$$

in which a is a constant that determines the mesh distribution. The larger a is, the smaller the mesh size becomes near the walls. Here a in the x- and y-directions is set to be 2 and 3.5, respectively. The grid points used in the discretization of spatial space are also listed in Table 1. Independence of the results on the discretized molecular velocity and spatial spaces given in Table 1 has been carefully confirmed for our simulations.

The computational time step in the DUGKS is solely determined by the Courant-Friedrichs-Lewy (CFL) condition [35],
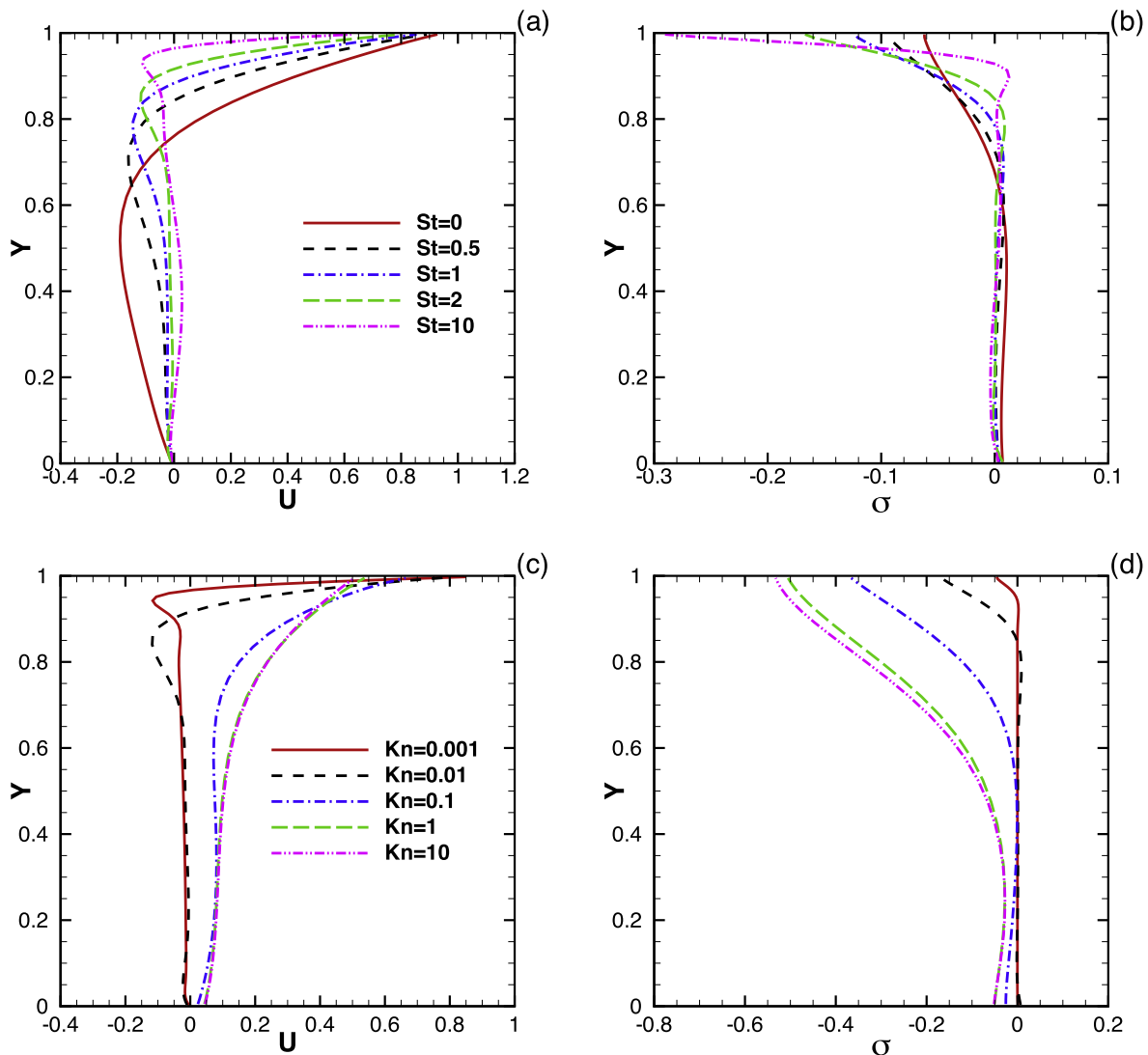
Fig. 2. The horizontal velocity U and the shear stress σ_{xy} along the line $x = 0.5$ for Kn = 0.01 at various St (top row), and for St = 2 at various Kn (bottom row). The shear stress profiles in (b) and (d), respectively, share the same legend as the velocity in (a) and (c). Here $t/T_s = 0$ and Ma = 0.1.

$\Delta t = \eta \Delta x_{min}/\xi_{max}$, where η is the CFL number, Δx_{min} is the minimum mesh size, and ξ_{max} is the maximum discretized molecular velocity. Note that the DUGKS has a distinguished performance in robustness [36,37], therefore, a relatively large CFL number can be used to reduce the computational time. In all the simulations, the CFL number $\eta \approx 0.5$ is set to satisfy $n\Delta t = \pi, n \in \mathbb{Z}^{+}$.

The accuracy of the DUGKS has been extensively demonstrated in the previous studies e.g. [24,36–39]. In particular, the capacity of DUGKS for the oscillatory rarefied flow has been proven in our recent study [6,28]. It should be emphasized that, the primary reason for adopting the DUGKS is that, different from the traditional DVM, the grid size in the DUGKS is not necessary to be smaller than the mean free path of gas molecules in the slip and continuum regimes [32], which allows the DUGKS to use much fewer grid points than the traditional DVM in describing the slip and continuum flows [24]. For example, as the Knudsen number changes from 10 to 0.001, the ratio of gas mean free path to the average mesh size varies widely from 640 to 0.064.

4. Results and discussion

Numerical simulations are performed by the DUGKS covering a wide range of the Knudsen numbers, the Strouhal numbers, and the Mach numbers, which describe the role of gas rarefaction,

oscillation frequency, and flow nonlinearity, respectively. The diffuse boundary condition is applied for gas-wall interactions [6].

For this unsteady problem, the flow converges to a time-periodic steady flow after a few periods of oscillation. The flow field is regarded as time-period flow steady-state, if the following criteria is satisfied:

$$\epsilon = \frac{\sum \|\boldsymbol{u}(nT_s) - \boldsymbol{u}((n-1)T_s))\|_1}{\sum \|\boldsymbol{u}(nT_s)\|_1} < 10^{-7}, n \in \mathbb{Z}^{+}, \tag{10}$$

where the summarization is taken over the whole flow field, $T_s = 2\pi/\omega$ is the oscillatory period of the lid, and n is number of the oscillatory period. In what follows, the results are prepared in a time-period steady-state unless otherwise stated. In addition, the velocity, temperature, shear stress, and heat flux are, respectively, normalized by the $U_0, T_w, \rho_0 RT_w U_0/v_m$ and $\rho_0 RT_w U_0$, with the reference density ρ_0 being set to 1. The height of the cavity is set to $H = 1$ for clarity.

4.1. Flow characteristics

Flow velocity and shear stress, which play an important role in determining the heat transfer mechanism, are first investigated at $t/T_s = 0$ and $Ma = 0.1$. Fig. 2(a) and Fig. 2(b) show the profiles of horizontal velocity and shear stress along the vertical centerline

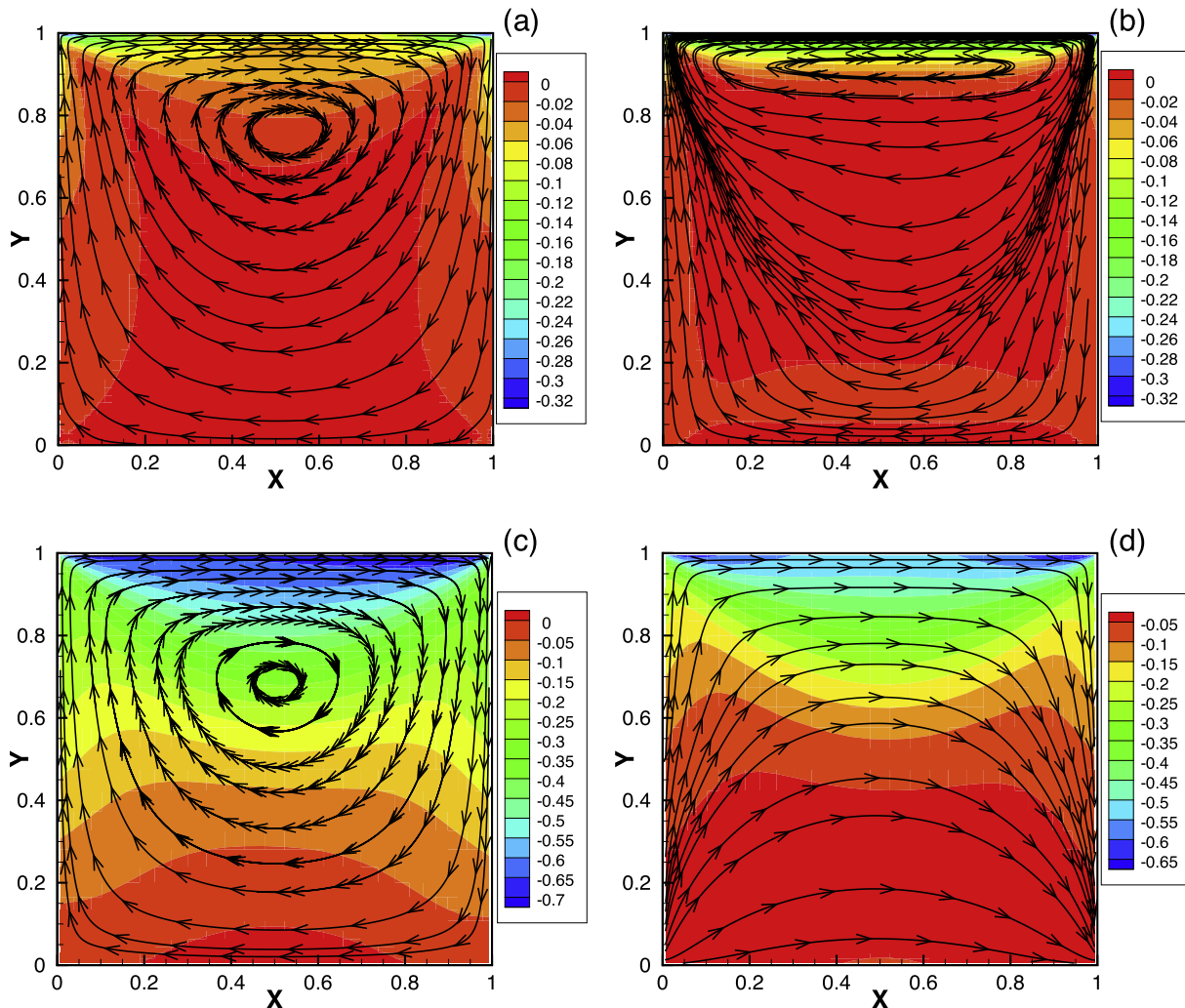

Fig. 3. Contours of the shear stress overlaid by the streamlines of the velocity for *Kn* = 0.01 (top row) and *Kn* = 10 (bottom row), with *St* = 0 (left column) and *St* = 2 (right column). Here *t/T*$_s$ = 0 and *Ma* = 0.1.

of $x = 0.5$ for $Kn = 0.01$, at different values of St. It is clear to see that the magnitude of shear stress exerting on the oscillation lid is proportional to the difference of velocity between the oscillating lid and the flow on the lid. As St increases, a larger magnitude of the shear stress on the lid is observed in Fig. 2(b), because of the reducing flow velocity there, see Fig. 2(a). However, for larger Knudsen numbers ($Kn \geqslant 0.1$), it was reported that the velocity and the Strouhal number show no general dependency [5]. In addition, the velocity (shear stress) near the moving lid at $x = 0.5$ reduces (increases) rapidly with St. It has been shown in the analysis of one-dimensional flow that a new length scale, i.e. the penetration depth, is created for the oscillatory Couette flow [3]. Here, we can define an analogical length scale as the distance from the moving wall to the position where the velocity decays to 10% of its excitation value (U_0). It is noticed that the penetration depth along the vertical centerline $x = 0.5$ decreases with increasing St, see Fig. 2(a).

The flow velocity and shear stress along the centerline of $x = 0.5$ for $St = 2$, with Kn from 0.001 to 10, are presented in Fig. 2(c) and Fig. 2(d), respectively. As expected, when Kn decreases, the horizontal velocity U on the lid increases, until reaching the no-slip limit $U = U_0$ at $Kn = 0.001$. In addition, negative minimum U is observed near the oscillating lid for $Kn = 0.001$ and 0.01, indicating that a vortex emerges there, as shown in Fig. 3(c). In Fig. 2(c), the location of the minimum U for a smaller Kn is found to be closer to the oscillating lid as well.

To further elaborate the above observations, the shear stress contours overlaid by the velocity streamlines for $Kn = 0.01$ and 10, with $St = 0$ and 2, are illustrated in Fig. 3. As expected, for $Kn = 0.01$, the vortex appears in both non-oscillatory and oscillatory flows, and location of the vortex center in the oscillatory flow is closer to the lid than that of the non-oscillatory one. However, for $Kn = 10$, a primary vortex emerges only in the non-oscillatory flow.

Finally, the velocity magnitude contours overlaid by the streamlines of velocity for $Kn = 0.1$ and $Kn = 1$ during the first quarter of the oscillation period are depicted in Fig. 4. When $t/T_s = 0$, the driving velocity $U_w = U_0$, the intense movements occur near the oscillating lid, where the streamlines are almost parallel to the moving lid. As U_w is reduced to about $0.31U_0$ at $t/T_s = 0.2$, for both $Kn = 0.1$ and 1, the flow penetrates deeper, a primary vertex emerges in the upper region of the cavity as well. Eventually, for $U_w = 0$ at $t/T_s = 0.25$, the regions, where the velocity magnitude is maximum, appear symmetrically along the vertical centerline of the cavity. Meanwhile, for $Kn = 1$, the vertex completely disappears, see Fig. 4(f).

4.2. Thermal characteristics

Fig. 5 shows the temperature field overlaid by the heat flux streamlines at $t/T_s = 0$ for $Kn = 0.01$, 0.1, 1, and 10, and $St = 0$, 0.5, 1, and 2. The Mach number is set to 0.1. We notice that, the cold and hot regions are normally located at the top left and right corners of the cavity, respectively. It is well recognized that for a low-speed lid-driven rarefied cavity flow, the anti-Fourier heat transfer, i.e. the heat transferring from the cold region to the hot one, is dominant, which has been extensively reported in the literatures [19,40–43]. We can see from the first column of Fig. 5 that when $St = 0$, even for a very small Knudsen number $Kn = 0.01$, the cold-to-hot heat transfer prevails inside the cavity, even though the heat transferring from the hot region (top-left corner) to the cold one (top-right corner) also takes place in the bottom left side of the cavity. As St is increased to 0.5, the hot-to-cold heat transfer becomes dominant at the cavity center, see Fig. 5(a2). Thereafter, when $St = 1$ (Fig. 5(a3)), the domain of hot-to-cold heat transfer is expanded to the middle and bottom of the cavity. Eventually, when $St = 2$ (Fig. 5(a4)), the hot-to-cold heat transfer almost dominates the whole cavity, except the two top corners, where the non-
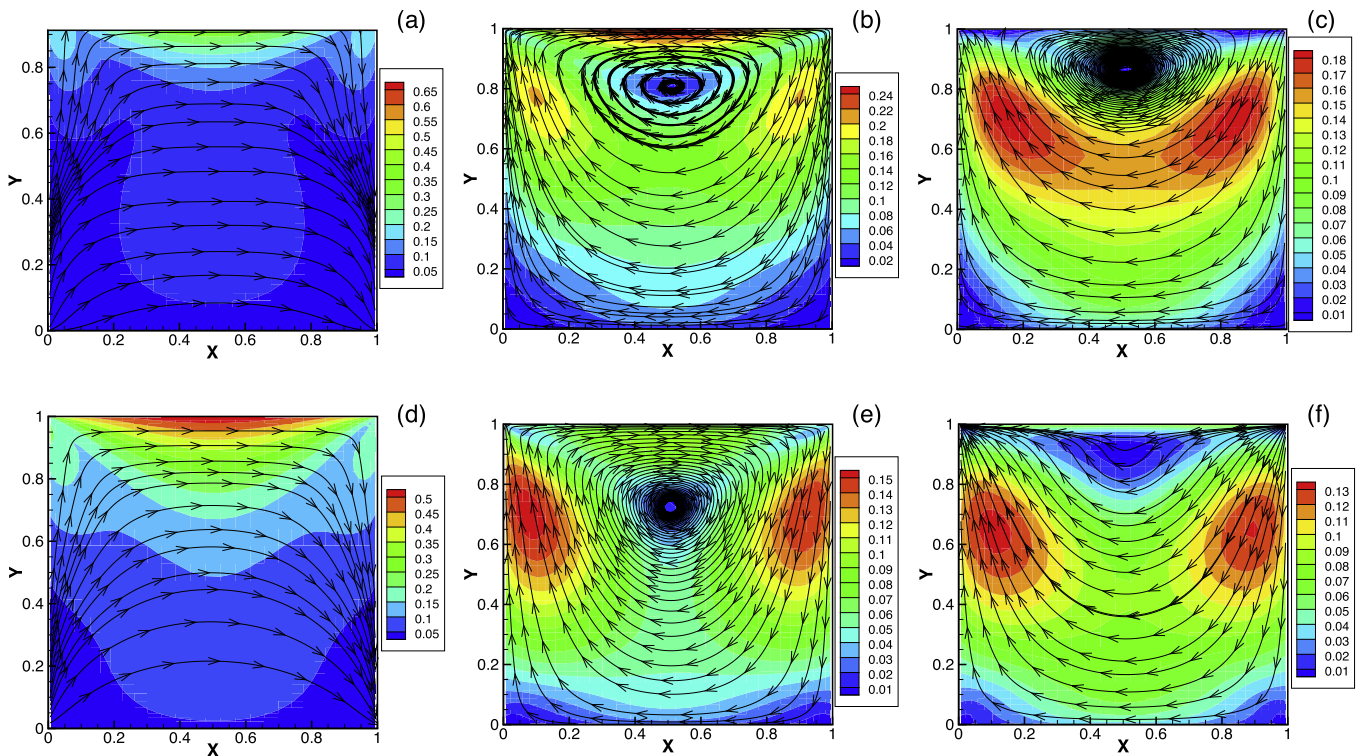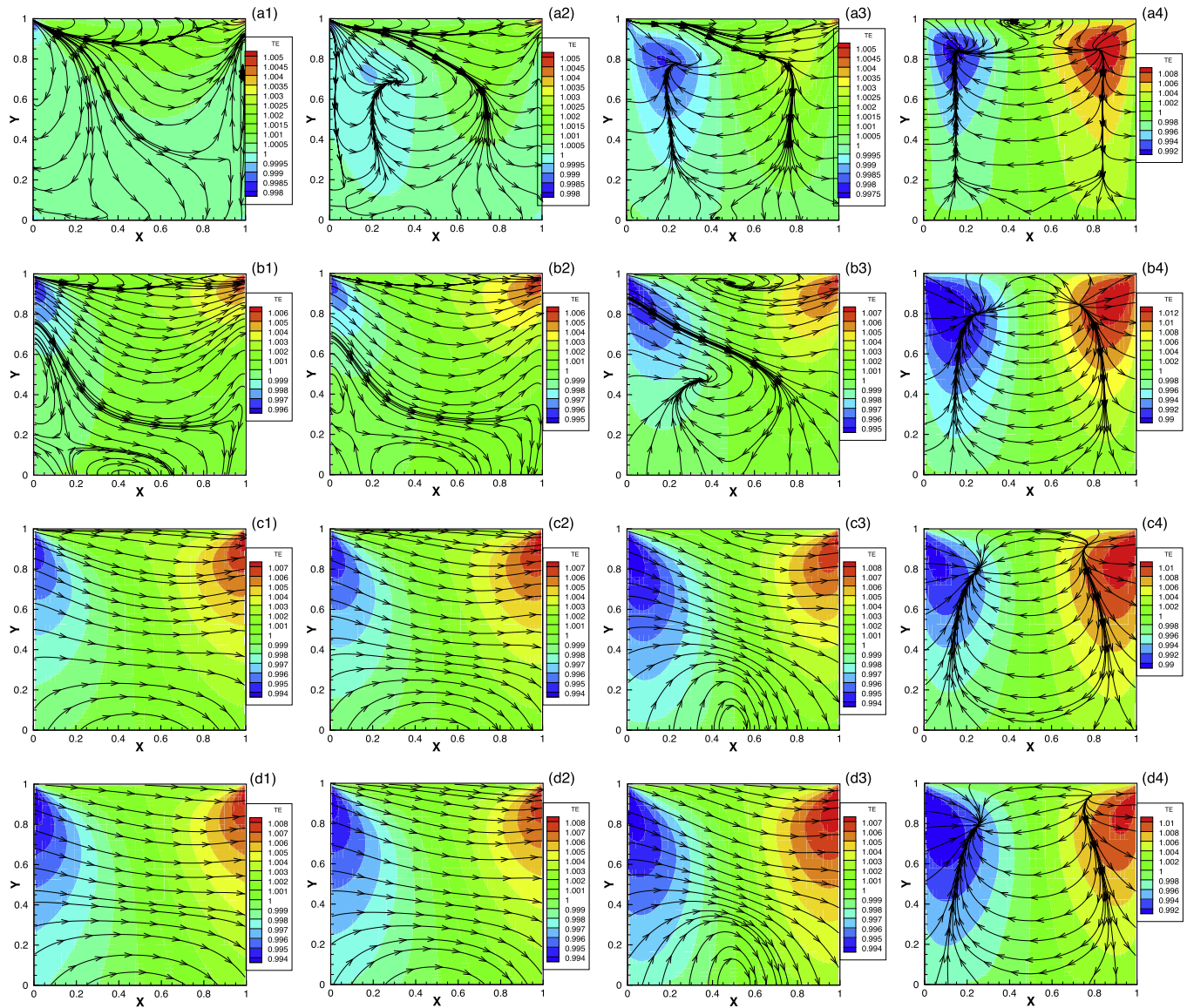

Fig. 4. Contours of the velocity magnitude overlaid by the velocity streamlines for $Kn = 0.1$ (top row) and $Kn = 1$ (bottom row), at $t/T_s = 0$, 0.2, and 0.25 (from left to right column). The Mach number is set to be 0.1.

Fig. 5. Contours of the temperature overlaid by the streamlines of heat flux for $Kn = 0.01, 0.1, 1$, and 10 (from top to bottom row), at $St = 0, 0.5, 1$, and 2 (from the left to right column), when $t/T_s = 0$ and $Ma = 0.1$.

equilibrium effects due to intensive gas-wall interactions are strong. The similar phenomena are also observed for the cases of $Kn = 0.1$, 1, and 10.

On the other hand, as the Knudsen number increases, the Strouhal number, at which the heat transfer pattern is reversed, i.e. transferring from cold-to-hot to hot-to-cold, becomes larger. For instance, when $St = 1$, the hot-to-cold heat transfer is dominant for $Kn = 0.01$, vice versa for $Kn = 1$, see Fig. 5(a3) and Fig. 5(c3). However, when $St = 2$, for all the Knudsen numbers, the hot-to-cold heat transfer prevails. These results indicate that, the oscillation of lid is able to change the heat transfer mechanism, such that the hot-to-cold heat transfer could be dominant in a highly rarefied flow, when the oscillating frequency of the lid is sufficiently high.

Different from the Fourier law in the framework of continuum theory, the gas kinetic theory can consider the rarefaction effect on heat transfer inside a lid-driven cavity. For a moderate Kn, the heat flux can be described by the regularized 13 moment equations as [42,40]:

$$Q_i = -\frac{15}{4}\mu\frac{\partial T}{\partial x_i} - \frac{3}{2}\frac{\mu}{p}T\frac{\partial\sigma_{ik}}{\partial x_k}, i \in \{x, y\}, \tag{11}$$

where the gradient of shear stress σ can also be represented by the second derivative of velocity, according to the Burnett equations [40,42]. The component of heat flux due to temperature gradient and the one due to shear stress gradient are plotted in Fig. 6, which confirms that the derivative of temperature governs the hot-to-cold heat transfer, while the shear stress gradient is responsible to the cold-to-hot heat flow. From Fig. 6(a) and Fig. 6(b), combining with Fig. 5(b1), it is noticed that, the heat transfer due to the gradient of shear stress dominates at $St = 0$. However, at $St = 2$, the heat transfer caused by temperature gradient in turn prevails inside the cavity, see Fig. 5(b4), Fig. 6(c) and Fig. 6(d).

The above observations can be qualitatively interpreted as follows: the lid oscillation can enhance the strength of shear motions inside the cavity, more heat is therefore generated through viscous dissipation. For the lid-driven cavity flow ($St = 0$), the moving lid with a small velocity ($Ma = 0.1$) induces a temperature field with a small variation, indicating a small local temperature gradient inside the cavity. Therefore, the contribution of shear stress gradients to heat flux is more significant than that due to the temperature gradient, which leads to cold-to-hot heat transfer. However, as the oscillation frequency increases, more heat is generated by the
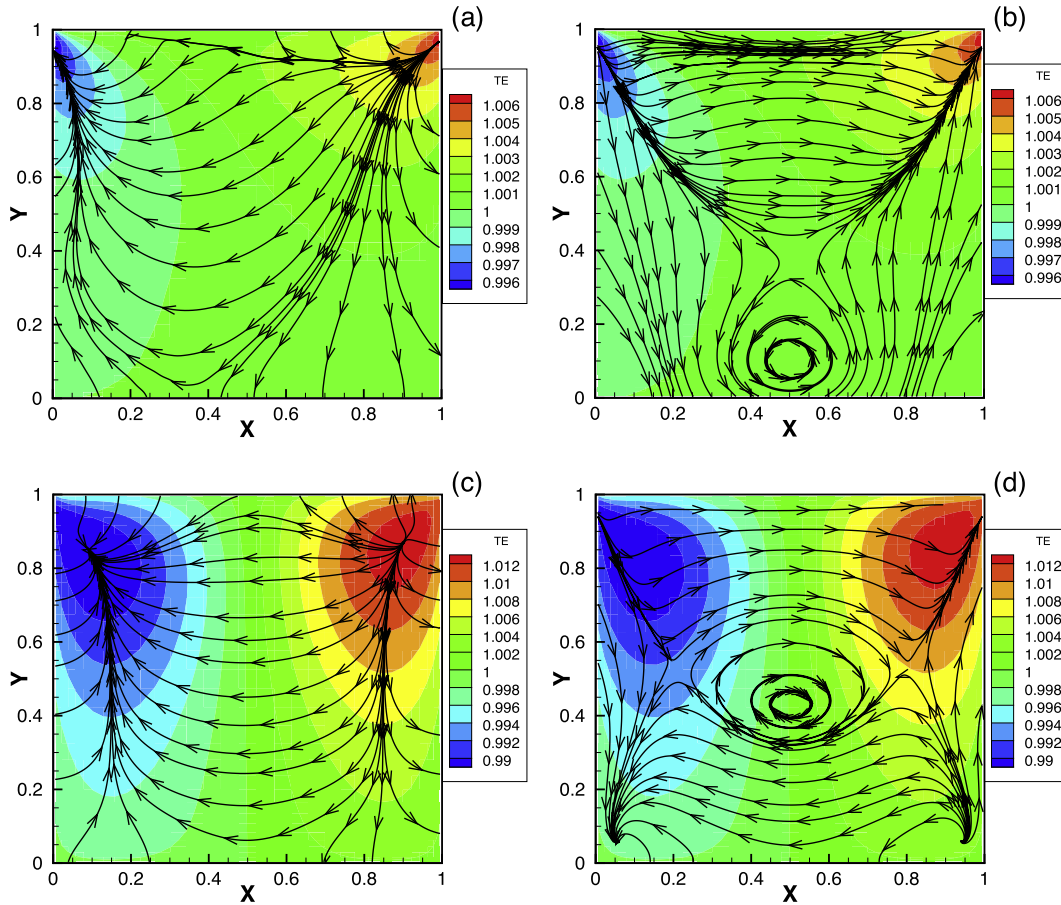
Fig. 6. Contours of the temperature overlaid by the streamlines of $\frac{\partial T}{\partial x_i}$ (a, c) and $\frac{\partial \sigma_{xy}}{\partial x_i}$ (b, d), for $St = 0$ (a, b) and $St = 2$ (c, d), at $t/T_s = 0$, $Kn = 0.1$ and $Ma = 0.1$. Note that $\frac{\partial \sigma_{xx}}{\partial x_i}$ and $\frac{\partial \sigma_{yy}}{\partial x_i}$ in this case can be neglected [40].

intense viscous dissipation, as a result, the variational range of the temperature is extended. Meanwhile, the hot and cold regions move toward the cavity center, which leads to a larger gradient of temperature there. When the oscillation frequency reaches a certain value, the hot-to-cold heat flux, which is proportional to the negative gradient of temperature, could surpass the cold-to-hot transfer associated with the gradient of the shear stress, as observed from the last column of Fig. 5. However, in the vicinity of the top corners, the gradient of shear stress is large, the cold-to-hot heat transfer therefore still dominates.

It is known that the nonlinearity of flow field can also affect heat transfer inside the cavity [6,19]. In order to elaborate the combined effect of lid-oscillation and gas rarefaction, we illustrate the temperature contours and the heat flux streamlines in Fig. 7 where Kn ranges from 0.001 to 1, $St = 0$ and 2, and $Ma = 1$ (producing a nonlinear flow field). Note that the heat transfer for $Kn = 10$ is similar to that of $Kn = 1$, so the results of $Kn = 10$ are not presented here. As we see from Fig. 7(a) and Fig. 7(b), for $Kn = 0.001$, the directions of heat flux are strictly perpendicular to the isotherms. That is to say, heat transfer satisfies the conventional Fourier law. The similar phenomena are observed from Fig. 7(c) and Fig. 7(d) for $Kn = 0.01$, in which the Fourier heat transfer still prevails inside the cavity, even though the flow is in the slip regime. Furthermore, for $Kn = 0.1$, when $St = 0$, even though the predominant heat transfer is hot-to-cold, see Fig. 7(e), the heat flux streamlines are not strictly perpendicular to the isotherms. When St is increased to 2, the heat transfer in the lower part of the cavity seems to satisfy the Fourier law, see Fig. 7(f). It is also noticed that when $St = 0$, the directions of heat transfer near the wall boundaries are from the gas to the wall, whereas when $St = 2$, it is from the wall to the gas near the left vertical wall. This is because the temperature inside a non-oscillatory cavity is overall higher than the wall temperature, while a cold region with the temperature being smaller than T_w is developed by a strong flow expansion (cooling effect) inside an oscillatory cavity.

In essence, temperature represents the total internal energy, which can be transformed from the kinetic energy through viscous dissipation. Therefore, the heat generation inside the cavity depends on not only the degree of gas rarefaction and velocity amplitude, but also the oscillation frequency of the driven lid. A higher speed on the lid indicates a larger input of the kinetic energy, thus increases internal energy in the cavity. Similarly, a higher oscillation frequency could induce more intense shear motion to generate more heat. Meanwhile, the less gas rarefaction is, the more frequent collisions of gas molecules are, leading to more heat generation. The interplay of these factors are responsible to the above complex phenomena.

4.3. The average Nusselt number on the oscillating lid

The heat transfer is characterized quantitatively by the Nusselt number (Nu), which is a measure of the relative strength of the convection and conduction processes. Specifically, the heat transfer is dominated by the conduction in the flow domain where $Nu < 1$, and by the convection as $Nu > 1$. In this work, of particular interest is the average Nusselt number Nu_a on the oscillating lid, which can reveal the dominant heat transfer behavior of the flow
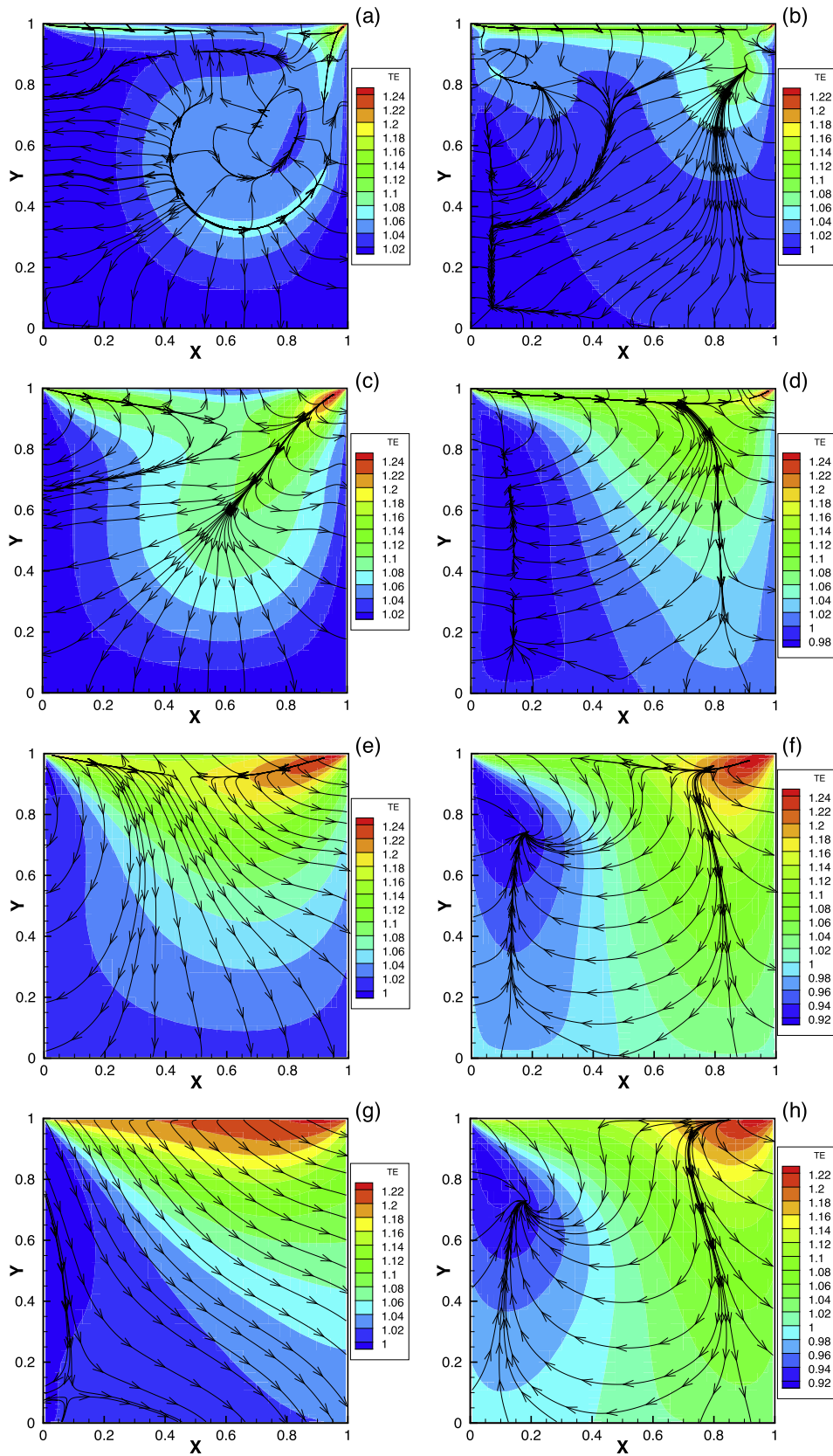
Fig. 7. Contours of the temperature overlaid by the streamlines of heat flux for *Kn* = 0.001, 0.01, 0.1, and 1 (from top row to bottom row), and *St* = 0 (left column) and 2 (right column). Here $t/T_s = 0$ and *Ma* = 1.
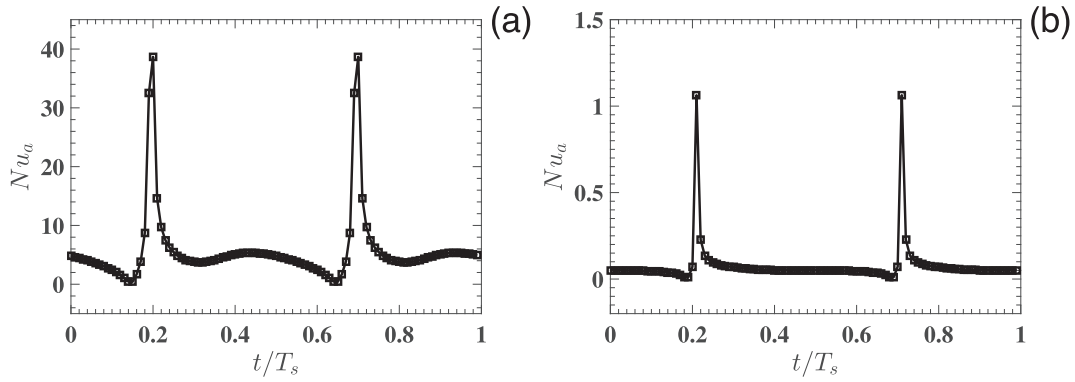
Fig. 8. Evolution of the average Nusselt number Nu_a during one-period of the oscillation for (a): $Kn = 0.1$ and (b) $Kn = 1$, with $Ma = 0.1$.
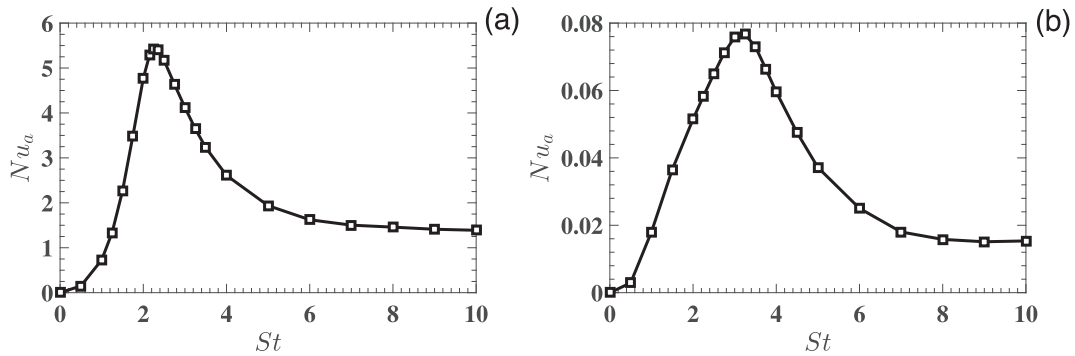

Fig. 9. Variation of the average Nusselt number Nu_a with the Strouhal number St for (a): $Kn = 0.1$ and (b) $Kn = 1$, when $t/Ts = 0$ and $Ma = 0.1$.

near the isothermal lid. The average Nusselt number Nu_a is defined as [44]

$$Nu_a = \frac{1}{H} \int_0^H Nu(x, y = H)dx, \quad \text{with } Nu(x, y = H) = \frac{Q_y(x, y = H)H}{\kappa(T_w - T_b)},$$
(12)

where κ is the gas thermal conductivity, Q_y is the heat flux along the vertical direction, and T_b is the bulk temperature inside the cavity defined as [44]

$$T_b = \frac{\int_A \rho UTdA}{\int_A \rho UdA},$$
(13)

where A is the whole domain of the cavity, and U is the velocity in x-direction. Note that because the heat flux is scaled by $\rho_0 RT_w U_0$, the difference of the average Nusselt number between the linear and nonlinear oscillations is so small that the effect of gas nonlinearity on Nu_a can be neglected. For example, for $St = 0$ and 4, the relative difference between the results of $Ma = 0.1$ and 1 is less than 1%. Therefore, we only present the results of $Ma = 0.1$ here.

Fig. 8 shows the evolution of Nu_a during one period for two typical Knudsen numbers, i.e. $Kn = 0.1$ and 1. It is found that the period of Nu_a is half of that of the oscillating lid. This is because the change of Nu_a is associated with the velocity magnitude and streamlines (see Fig. 4) inside the cavity, whose periods are half of the oscillation period [5,6]. In addition, two peaks of Nu_a appear at $t/T_s = 0.2$ and 0.7, suggesting the strong convection caused by the intensive flow at these times, which can be confirmed by the vortex currents shown in Fig. 4.

The variations of Nu_a with respect to St for $Kn = 0.1$ and 1 are depicted in Fig. 9, where $t/T_s = 0$. We note that as St increases, Nu_a first increases dramatically to a maximum at $St \approx 2.3$ and 3.3

for $Kn = 0.1$ and 1, respectively, then decreases rapidly to a limiting value when $St > 8$. It is interesting to note that, at approximately the same Strouhal number for the maximum Nu_a to appear, i.e. $St_a \approx 2.5$ and 3.5 respectively [5,6], the anti-resonance occurs and the damping force exerting on the lid reaches a local minimum. This is because the flow velocity along the oscillating lid reaches its maximum at the anti-resonance frequency, which induces the strongest convective heat transfer near the moving lid.

Table 2 summarizes the average Nusselt number Nu_a on the oscillating lid at different Kn and St. We find that Nu_a decreases with increasing Kn, which is similar to the observation in the micro-channel [44,45]. When the lid oscillation frequency and speed are fixed, increasing rarefaction will reduce gas bulk motion. So the heat convection becomes less significant. In addition, when $St = 0$ the heat convection near the driven lid is weak for all the Knudsen numbers, and the conduction absolutely dominates the heat transfer there. However, by enforcing an oscillation on the lid, even in a very small frequency, e.g. $St = 0.5$, the intensity of thermal convection relative to the conduction could be boosted for several orders of magnitude.

Table 2
The average Nusselt number Nu_a on the oscillating lid with different values of Kn and St, at $t/Ts = 0$.

St/Kn	0.001	0.01	0.1	1	10
0	8.7721e−03	3.4439e−03	5.7691e−04	1.3240e−06	3.4931e−07
0.5	7.7582	1.0065	1.4889e−01	2.9020e−03	1.3119e−03
1	43.885	4.1496	7.2916e−01	1.8029e−02	2.6743e−03
2	1381.2	2.5005	4.7717	5.1495e−02	7.2586e−03
10	173.94	30.673	1.3887	2.5027e−02	1.0593e−04

5. Conclusions

The flow and thermal characteristics of the oscillatory rarefied flow inside a square cavity have been systematically investigated on the basis of the gas-kinetic theory. We find that the oscillation frequency and speed of the lid can significantly change the heat transfer in the cavity. For example, in contrast to the cold-to-hot heat transfer observed in rarefied gas flow in a lid-driven cavity, the hot-to-cold transfer can prevail for the highly rarefied flows if the lid oscillates with sufficiently high frequency or speed. The thermal convection can be dramatically strengthened by enforcing an oscillation on the lid, so that the convective transfer may play a dominant role even for the moderately rarefied flows. As the oscillation frequency becomes larger, the average Nusselt number on the lid first increases to a maximum, then decreases to a limiting value. The oscillation frequency, at which the average Nusselt number is maximum, is almost the same as the anti-resonance frequency. In addition, the average Nusselt number on the lid is found to reduce with gas rarefaction.

Conflict of interest

The authors declared that there is no conflict of interest.

Acknowledgments

Appendix A. Supplementary material

Supplementary data associated with this article can be found, in the online version, at https://doi.org/10.1016/j.ijheatmasstransfer.2018.11.060.

References

[1] A. Beskok, G. Karniadakis, Microflows and Nanoflows: Fundamentals and Simulation. Interdisciplinary Applied Mathematics, Springer, 2005.
[2] F. Sharipov, D. Kalempa, Oscillatory Couette flow at arbitrary oscillation frequency over the whole range of the Knudsen number, Microfluid. Nanofluid. 4 (5) (2008) 363–374.
[3] J.H. Park, P. Bahukudumbi, A. Beskok, Rarefaction effects on shear driven oscillatory gas flows: a direct simulation Monte Carlo study in the entire Knudsen regime, Phys. Fluids 16 (2) (2004) 317–330.
[4] A. Frangi, A. Frezzotti, S. Lorenzani, On the application of the BGK kinetic model to the analysis of gas-structure interactions in MEMS, Comput. Struct. 85 (11) (2007) 810–817.
[5] L. Wu, J.M. Reese, Y. Zhang, Oscillatory rarefied gas flow inside rectangular cavities, J. Fluid Mech. 748 (2014) 350–367.
[6] P. Wang, L. Zhu, W. Su, L. Wu, Y. Zhang, Nonlinear oscillatory rarefied gas flow inside a rectangular cavity, Phys. Rev. E 97 (4) (2018) 043103.
[7] D. Kalempa, F. Sharipov, Sound propagation through a rarefied gas confined between source and receptor at arbitrary Knudsen number and sound frequency, Phys. Fluids 21 (10) (2009) 103601.
[8] F. Sharipov, Rarefied Gas Dynamics: Fundamentals for Research and Practice, John Wiley & Sons, 2015.
[9] S. Stefanov, P. Gospodinov, C. Cercignani, Monte Carlo simulation and Navier–Stokes finite difference calculation of unsteady-state rarefied gas flows, Phys. Fluids 10 (1) (1998) 289–300.
[10] N.G. Hadjiconstantinou, Sound wave propagation in transition-regime micro- and nanochannels, Phys. Fluids 14 (2) (2002) 802–809.
[11] J.H. Park, S.W. Baek, S.J. Kang, M.J. Yu, Analysis of thermal slip in oscillating rarefied flow using DSMC, Numer. Heat Transf.: Part A: Appl. 42 (6) (2002) 647–659.
[12] J.H. Park, S.W. Baek, Investigation of influence of thermal accommodation on oscillating micro-flow, Int. J. Heat Mass Transf. 47 (6) (2004) 1313–1323.
[13] N.G. Hadjiconstantinou, A.L. Garcia, Molecular simulations of sound wave propagation in simple gases, Phys. Fluids 13 (4) (2001) 1040–1046.
[14] D.R. Emerson, X.-J. Gu, S.K. Stefanov, S. Yuhong, R.W. Barber, Nonplanar oscillatory shear flow: from the continuum to the free-molecular regime, Phys. Fluids 19 (10) (2007) 107105.
[15] T. Doi, Numerical analysis of oscillatory Couette flow of a rarefied gas on the basis of the linearized Boltzmann equation, Vacuum 84 (5) (2009) 734–737.
[16] T. Tsuji, K. Aoki, Gas motion in a microgap between a stationary plate and a plate oscillating in its normal direction, Microfluid. Nanofluid. 16 (6) (2014) 1033–1045.
[17] L. Wu, Sound propagation through a rarefied gas in rectangular channels, Phys. Rev. E 94 (5) (2016) 053110.
[18] S. Hutcherson, W. Ye, On the squeeze-film damping of micro-resonators in the free-molecule regime, J. Micromech. Microeng. 14 (12) (2004) 1726.
[19] B. John, X.-J. Gu, D.R. Emerson, Investigation of heat and mass transfer in a lid-driven cavity under nonequilibrium flow conditions, Numer. Heat Transf. Part B: Fundam. 58 (5) (2010) 287–303.
[20] C. Liu, K. Xu, Q. Sun, Q. Cai, A unified gas-kinetic scheme for continuum and rarefied flows IV: full Boltzmann and model equations, J. Comput. Phys. 314 (2016) 305–340.
[21] T. Xiao, Q. Cai, K. Xu, A well-balanced unified gas-kinetic scheme for multiscale flow transport under gravitational field, J. Comput. Phys. 332 (2017) 475–491.
[22] T. Xiao, K. Xu, Q. Cai, T. Qian, An investigation of non-equilibrium heat transport in a gas system under external force field, Int. J. Heat Mass Transf. 126 (2018) 362–379.
[23] L. Yang, C. Shu, W. Yang, J. Wu, An implicit scheme with memory reduction technique for steady state solutions of DVBE in all flow regimes, Phys. Fluids 30 (4) (2018) 040901.
[24] P. Wang, M.T. Ho, L. Wu, Z. Guo, Y. Zhang, A comparative study of discrete velocity methods for low-speed rarefied gas flows, Comput. Fluids 161 (2017) 33–46.
[25] K. Xu, Direct Modeling for Computational Fluid Dynamics: Construction and Application of Unified Gas-kinetic Schemes, World Scientific, 2014.
[26] N.G. Hadjiconstantinou, Oscillatory shear-driven flows in the transition and free-molecular-flow regimes, Phys. Fluids 17 (10) (2005) 100611.
[27] K. Aoki, S. Kosuge, T. Fujiwara, T. Goudon, Unsteady motion of a slightly rarefied gas caused by a plate oscillating in its normal direction, Phys. Rev. Fluids 2 (1) (2017) 013402.
[28] P. Wang, W. Su, Y. Zhang, Oscillatory rarefied gas flow inside a three dimensional rectangular cavity, Phys. Fluids 30 (10) (2018) 102002.
[29] S. Naris, D. Valougeorgis, The driven cavity flow over the whole range of the Knudsen number, Phys. Fluids 17 (9) (2005) 097106.
[30] E. Shakhov, Generalization of the Krook kinetic relaxation equation, Fluid Dyn. 3 (5) (1968) 95–96.
[31] Z. Guo, R. Wang, K. Xu, Discrete unified gas kinetic scheme for all Knudsen number flows. II. Thermal compressible case, Phys. Rev. E 91 (3) (2015) 033313.
[32] K. Xu, C. Liu, A paradigm for modeling and computation of gas dynamics, Phys. Fluids 29 (2017) 026101.
[33] L. Wu, J.M. Reese, Y. Zhang, Solving the Boltzmann equation deterministically by the fast spectral method: application to gas microflows, J. Fluid Mech. 746 (2014) 53–84.
[34] W. Su, S. Lindsay, H. Liu, L. Wu, et al., Comparative study of the discrete velocity and lattice boltzmann methods for rarefied gas flows through irregular channels, Phys. Rev. E 96 (2) (2017) 023309.
[35] Z. Guo, K. Xu, R. Wang, Discrete unified gas kinetic scheme for all Knudsen number flows: low-speed isothermal case, Phys. Rev. E 88 (3) (2013) 033305.
[36] P. Wang, L. Zhu, Z. Guo, K. Xu, A comparative study of LBE and DUGKS methods for nearly incompressible flows, Commun. Comput. Phys. 17 (03) (2015) 657–681.
[37] L. Zhu, P. Wang, Z. Guo, Performance evaluation of the general characteristics based off-lattice Boltzmann scheme and DUGKS for low speed continuum flows, J. Comput. Phys. 333 (2017) 227–246.
[38] Y. Bo, P. Wang, Z. Guo, L.-P. Wang, DUGKS simulations of three-dimensional Taylor–Green vortex flow and turbulent channel flow, Comput. Fluids 155 (2017) 9–21.
[39] P. Wang, L.-P. Wang, Z. Guo, Comparison of the lattice Boltzmann equation and discrete unified gas-kinetic scheme methods for direct numerical simulation of decaying turbulent flows, Phys. Rev. E 94 (4) (2016) 043304.
[40] A. Mohammadzadeh, E. Roohi, H. Niazmand, S. Stefanov, R.S. Myong, Thermal and second-law analysis of a micro- or nanocavity using direct-simulation Monte Carlo, Phys. Rev. E 85 (5) (2012) 056310.
[41] J.-C. Huang, K. Xu, P. Yu, A unified gas-kinetic scheme for continuum and rarefied flows ii: multi-dimensional cases, Commun. Comput. Phys. 12 (3) (2012) 662–690.
[42] A. Rana, M. Torrilhon, H. Struchtrup, A robust numerical method for the R13 equations of rarefied gas dynamics: application to lid driven cavity, J. Comput. Phys. 236 (2013) 169–186.
[43] L. Yang, C. Shu, J. Wu, Y. Wang, Numerical simulation of flows from free molecular regime to continuum regime by a DVM with streaming and collision processes, J. Comput. Phys. 306 (2016) 291–310.
[44] N.G. Hadjiconstantinou, O. Simek, Constant-wall-temperature Nusselt number in Micro and Nano-channels, J. Heat Transf. 124 (2) (2002) 356–364.
[45] S. Colin, Gas microflows in the slip flow regime: a critical review on convective heat transfer, J. Heat Transf. 134 (2) (2012) 020908.